

Journal Pre-proof

Amine-functionalized hollow mesoporous nano-bowl with bulky acid-imprinted free space around base sites and DMF-annealed mesoporous channels as an efficient solid base catalyst

Li Zhang (Data curation) (Visualization) (Investigation), Jianing Zhang (Formal analysis) (Software), Shuai Wei (Validation) (Resources), Shan Li (Resources), Xuebing Ma (Conceptualization) (Methodology) (Writing - review and editing) (Project administration) (Funding acquisition)



PII: S0926-860X(20)30153-8
DOI: <https://doi.org/10.1016/j.apcata.2020.117560>
Reference: APCATA 117560

To appear in: *Applied Catalysis A, General*

Received Date: 2 February 2020
Revised Date: 1 April 2020
Accepted Date: 9 April 2020

Please cite this article as: Zhang L, Zhang J, Wei S, Li S, Ma X, Amine-functionalized hollow mesoporous nano-bowl with bulky acid-imprinted free space around base sites and DMF-annealed mesoporous channels as an efficient solid base catalyst, *Applied Catalysis A, General* (2020), doi: <https://doi.org/10.1016/j.apcata.2020.117560>

This is a PDF file of an article that has undergone enhancements after acceptance, such as the addition of a cover page and metadata, and formatting for readability, but it is not yet the definitive version of record. This version will undergo additional copyediting, typesetting and review before it is published in its final form, but we are providing this version to give early visibility of the article. Please note that, during the production process, errors may be discovered which could affect the content, and all legal disclaimers that apply to the journal pertain.

© 2020 Published by Elsevier.

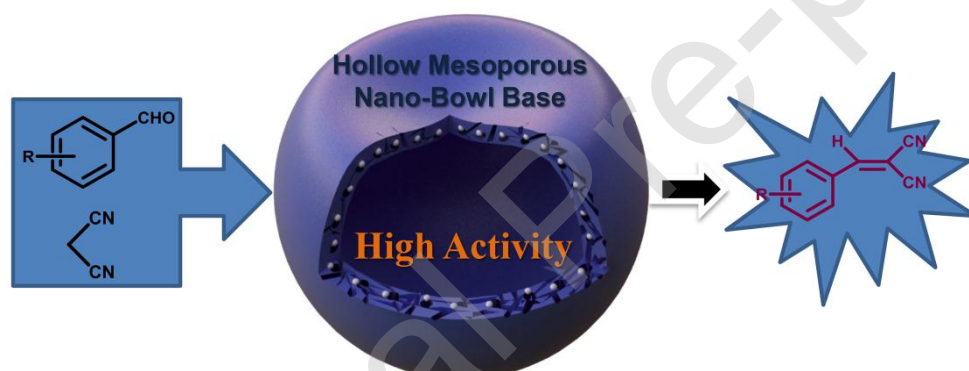
Amine-functionalized hollow mesoporous nano-bowl with bulky acid-imprinted free space around base sites and DMF-annealed mesoporous channels as an efficient solid base catalyst

Li Zhang, Jianing Zhang, Shuai Wei, Shan Li and Xuebing Ma* zcj123@swu.edu.cn

College of Chemistry and Chemical Engineering, Southwest University, Chongqing, 400715, P. R. China

* Corresponding author.

Graphical Abstract



Well-shaped nanobowl-like solid amine base with a hollow interior, mesoporous shell, free space around amine sites, inter-connected channels, and thin shell displayed high catalytic activity in the Knoevenagel condensations of aromatic aldehydes with malononitrile.

Highlights

- Fabrication of hollow mesoporous nano-bowl solid base with high mass transfer
- Imprint of free space around base site by etching bulky organic acid template
- Construction of mesoporous channel by solvent annealing
- High catalytic activity in Knoevenagel condensation at room temperature

- Good reusability and restoration of solid amine base

Abstract

Tailoring free spaces around catalytic sites and constructing inter-connected channels between them are highly attractive for achieving easy accessibility of reactants to catalytic sites. In this study, a strategy for constructing free space around base sites through molecular imprinting and interconnected channel between them by solvent annealing was developed to achieve high reactant accessibility. The as-fabricated nanobowls with particle sizes of 345 nm were efficient solid bases with fast mass transfer owing to the characteristic architectural features, such as a thin shell thickness (30 nm), free space around the base centered at 4.0 nm, mesoporous channels (5-50 nm), and a hollow interior. The influence of porosity on catalytic behavior was investigated using Knoevenagel condensations, and was found to promote various aromatic aldehydes to afford products at room temperature in 84–98% yield within 2h. Furthermore, the catalyst reused ten times was able to be restored to obtain original high catalytic activity.

Keywords: Solid base; Knoevenagel condensation; Hollow mesoporous nanobowl; Molecular imprinting; Solvent annealing.

1. Introduction

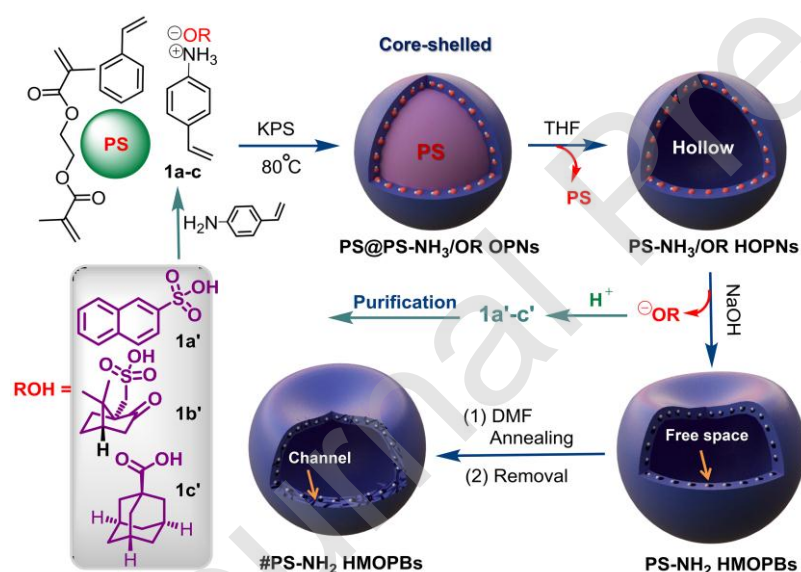
From the perspective of green and sustainable chemistry, solid base catalysts play an important role in catalyzing various reactions such as isomerization, hydrogenation, Tishchenko, Henry, Knoevenagel, and aldol reactions [1]. Various materials are used as supports for solid bases, ranging from inorganic materials, such as alumina, zeolites, and mesoporous silicas [2–4], to porous organic polymers and metal–organic frameworks [5]. With the development of synthetic methods and accurate characterization for solid catalysts, their applications to

industrial organic transformations for fine chemical production [1–4] and biomass conversion for biodiesel production [6–9] have attracted increasing attention.

Organic amines are attractive and readily available bases widely applied in base catalysis [10–12], metal coordination chemistry [13–15], and carbon capture in environmental science [16–18]. Owing to the increasing focus on green and sustainable chemistry, various types of solid materials, including organic, inorganic, and inorganic-organic hybrid materials, have been used as catalyst carriers to achieve the recovery and reuse of organic amines in heterogeneous base catalysis [19–27], and as solid supports to accomplish carbon capture and storage [28–30]. Inevitably, the question of how to improve the mass transfer of reactants [31–33] or adsorbates [34–36] in the frameworks of solid materials is a problem faced by all solid amines. To overcome the diffusion barrier of reactants inside catalyst carriers, high and tunable porosity is highly desirable for solid amines to achieve high catalytic performance in heterogeneous catalysis. Accordingly, organic amines have been grafted on ordered mesoporous silicas [37–40] and MOFs with uniform mesopores [5, 41–45] to enhance the in-pore molecule diffusion of reactants. Furthermore, the in-pore molecular diffusion of reactants in the solid skeleton is closely related to the hydrophilicity/hydrophobicity of the pore wall [46–49], seepage distance of the reactants [50–54] and hollow interior of the catalyst [55–61]. The empty space around a catalytic site is also an important contributor to the in-pore molecular diffusion of reactants inside solid materials, providing enough free space for reactants to access the catalytic site surface [62, 63]. To date, constructing free space around base sites to improve the accessibility of reactants/adsorbates to the base site surfaces in heterogeneous base catalysis and environmental science has been seldom explored.

In this study, based on the chemical reactivity of amino group for salt formation with organic acids, and the solubility and swellability of cross-linked and linear polystyrene, novel solid amine bases #PS-NH₂ HMOPBs (PS, polystyrene; HMOPBs, hollow mesoporous organic polymeric nanobowls) with a well-shaped polystyrene

nanobowl as the catalyst carrier with a hollow interior, free spaces around the amine sites and mesoporous channels in the shell were developed. These #PS-NH₂ HMOPBs were prepared by coating the surface of spherical PS with the ethylene glycol dimethylacrylate (EGDMA)-cross-linked copolymer of styrene and amine salts of 4-aminomethyl styrenes (1a-c), and then etching the PS core and bulky organic acid template (1a'-c') to fabricate nanobowls with a hollow interior and free space around the amine base. This was followed by swelling in DMF at 80 °C, annealing in liquid N₂, and removing frozen DMF using MeOH [64] to construct inter-connected mesoporous channels in the shell (Scheme 1). Owing to the hollow interior, thin shell, free space around amine sites, and mesoporous channel, the as-prepared solid amine #PS-NH₂ HMOPBs had ideal architectural features for reactants to access the base catalytic site surfaces and showed significantly enhanced catalytic activities in Knoevenagel condensations of aromatic aldehydes and malononitrile.



Scheme 1. Preparation of amine-functionalized hollow mesoporous organic polymeric nano-bowls #PS-NH₂ HMOPBs.

2. Experimental

2.1. Materials and characterization

Styrene was purified by distillation under reduced pressure before use. Polystyrene nanospheres (PS, $d = 285 \pm 15$ nm, $n = 100$) were prepared as cores according to the reference [61], whose SEM image and particle size distribution were shown in Fig. S1. 4-Vinyl benzylamine was synthesized according to the procedure shown in ESI#. The contrast solid amines, organic polymeric nanospheres (PS-NH₂ OPNs), and hollow organic polymeric nanospheres (PS-NH₂ HOPNs), were prepared according to the procedure (Scheme S1) in ESI#. The other chemicals were used as received without any further purification.

The chemical structures of products in Knoevenagel condensations were confirmed by ¹H NMR spectra on a Bruker av-600 NMR instrument, in which all chemical shifts were reported down-field in ppm relative to the hydrogen resonance of TMS. Elemental analysis was carried out on a vario Micro cube elemental analyzer. The morphology of sample was observed using SM-7800F scanning electron microscopy (SEM) and Tecnai G2 F20 transmission electron microscope (TEM), operated at 10 kV and 200 kV, respectively. N₂ adsorption–desorption isotherms were performed at 77.4 K on Autosorb-1 apparatus, in which samples were degassed at 105 °C for 12 h before measurement. The BET surface area was calculated from adsorption data in relative pressures P/P_0 (0.05–0.30), and the pore diameter distributions and pore volumes of samples were obtained from desorption branches using BJH method. FT-IR spectroscopy was performed on a Perkin-Elmer model GX spectrometer using KBr pellet. Knoevenagel condensation was monitored throughout by Agilent LC-1200 HPLC with a 210 nm UV-vis detector using Daicel Chiralpak chiral OD-H column (4.6 mm × 25 cm), eluting with *n*-hexane/*iso*-propanol (85/15) at a flow rate of 0.8 mL min⁻¹ at 20 °C.

2.2. Synthesis of 4-vinyl benzylamine salts

In round-bottom flask (100 mL), 4-vinyl benzylamine (0.80 g, 6.3 mmol) was dissolved in 20 mL of methanol, and then 15 mL of *iso*-propanol solution containing β -naphthalene sulfonic acid 1a' (1.31 g, 6.3 mmol) was added dropwise (about 1.5 h) at 0 °C. The precipitate was filtered and dried to afford white 4-vinyl benzylamine

naphthalene sulfonate 1a (2.0 g, 95%). $^1\text{H NMR}$ (600.0 MHz, DMSO-d_6): δ 8.17 (s, 4H), 7.97 (dd, $J = 5.8, 3.4$ Hz, 1H), 7.91 (dd, $J = 5.8, 3.4$ Hz, 1H), 7.88 (d, $J = 6$ Hz, 1H), 7.74 (d, $J = 6$ Hz, 1H), 7.54-7.52 (m, 2H), 7.50 (d, $J = 12$ Hz, 2H), 6.76-6.71 (m, 1H), 5.87(d, $J=18$ Hz, 1H), 5.29 (d, $J=12$ Hz, 1H), 4.03 (s, 2H).

When sulfonic acid 1a' was replaced by camphorsulfonic acid 1b' and adamantane formic acid 1c', yellow sulfonic amine salt 1b (2.1 g, 92%) and white carboxylic acid amine salt 1c (1.6 g, 80%) were also prepared according to the above-mentioned procedure. 1b: $^1\text{H NMR}$ (600 MHz, DMSO-d_6): δ 8.36 (s, 3H), 7.64 (d, $J = 6$ Hz, 2H), 7.58 (d, $J = 12$ Hz, 2H), 6.89 - 6.85 (m, 1H), 6.00 (d, $J = 18$ Hz, 1H), 5.42 (d, $J = 18$ Hz, 1H), 4.17-4.14 (m, 2H), 2.77 (m, 2H), 2.74 (s, 1H), 2.63 (s, 1H), 2.61 (s, 1H), 2.38 (d, $J = 18$ Hz, 1H), 1.49-1.39 (m, 4H), 1.30-1.24 (m, 1H). 1c: $^1\text{H NMR}$ (600 MHz, DMSO-d_6): δ 7.42 (d, $J = 6$ Hz, 2H), 7.33 (d, $J = 6$ Hz, 2H), 6.73-6.69 (m, 1H), 5.80 (d, $J = 18$ Hz, 1H), 5.22 (d, $J = 6$ Hz, 1H), 3.75 (s, 2H), 1.68-1.62 (m, 13H).

2.3. Preparation of hollow mesoporous organic polystyrene nano-bowls (#PS-NH₂ HMOPBs)

In N₂-filled three-necked round-bottom flask, PS nanospheres (0.25 g) were dispersed in 28 mL of 0.5 wt% PVA-containing mixed H₂O/DMSO (1:1, v/v), stirred at room temperature for 12 h, and added 4 mL of DMSO solution contained St (104 mg, 1.0 mmol), 1a (133 mg, 0.4 mmol), EGDMA (40 mg, 0.2 mmol), and 3 mL of aqueous potassium peroxydisulfate solution (KPS, 40 mg, 0.15 mmol) at 55 °C. After being stirred for 40 min, the well-dispersed emulsion was heated to 85 °C and stirred for 24 h. The cooled mixture was added 70 mL of ethanol, stirred for 30 min, and separated by centrifugation to afford core-shelled nanospheres PS@PS-NH₃/OR OPNs (365.0 mg). The obtained PS@PS-NH₃/OR OPNs (150.0 mg) were dispersed in 9 mL of THF, and stirred at room temperature for 12 h to remove the PS cores. The procedure was repeated two more times until the turbid phenomenon was not observed upon adding THF solution into water, indicating the complete removal of the PS cores. The isolated hollow nanospheres PS-NH₃/OR HOPNs was dealt with 9 mL of aqueous NaOH solution (2.0 mol L⁻¹) with stirring for 12 h to remove the imprinted molecule. The solids were further dealt with aqueous NaOH

solution two more times till no white solid was observed upon adding aqueous BaCl_2 solution. The solids were dried naturally to afford hollow mesoporous organic polymeric nanobowls PS-NH₂ HMOPBs (70.2 mg). Subsequently, PS-NH₂ HMOPBs (100 mg) was dispersed in 10 mL of DMF at 80 °C for 24 h, and transferred to liquid N₂ to freeze the reaction mixture. The frozen mixture was transferred to a refrigerator with -80 °C, and added 25 mL of CH₃OH to extract the frozen DMF molecules. The solids were dried under vacuum at room temperature to yield nanobowls #PS-NH₂ HMOPBs(80) (98.2 mg).

At DMF swelling temperature of 115 °C and 145 °C, other solid amines, designated as #PS-NH₂ HMOPBs(115) and #PS-NH₂ HMOPBs(145), were also prepared according to the above-mentioned procedure.

2.4. General procedure of Knoevenagel condensation

In a dried vial, benzaldehyde (106.0 mg, 1.0 mmol), malononitrile (80.0 mg, 1.2 mmol), #PS-NH₂ HMOPBs (61.2 mg, 0.05 mmol of amine) and ethanol (2 mL) were charged. Then, the reaction mixture was stirred at room temperature for 2 h. After the benzaldehyde was completely consumed, #PS-NH₂ HMOPBs was recovered by centrifugal separation, washed by ethanol, and directly reused in the following catalytic cycles. The centrifugate was purified by column chromatography on silica gel eluted with petroleum ether/diethyl ether (=10:1, v/v) to afford the white product (150.9 mg, 98%).

2.5. Restoration of #PS-NH₂ HMOPBs reused ten times

The 10th-reused #PS-NH₂ HMOPBs(80) (100 mg) was allowed to stir in 6 mL of aqueous HCl (1.0 mol L⁻¹) ethanol solution (1:1, v/v) at room temperature for 12 h and separated by centrifugation. The isolated #PS-NH₂ HMOPBs(80) was neutralized in 6 mL of aqueous NaOH (2.0 mol L⁻¹) ethanol solution (1:1, v/v) at room temperature for 12 h, separated by centrifugation, washed by distilled water to pH = 7, and dried naturally to afford restored #PS-NH₂ HMOPBs.

3. Results and discussion

3.1. Fabrication of well-shaped hollow mesoporous nanobowl

Theoretically, the mass transport of reactants in a porous spherical catalyst has been discussed in depth [65–67]. For first-order kinetics, the effectiveness factor (η) is given as a function of the Thiele modulus (ϕ_s) with constant concentration at the catalyst surface, as shown in equations (1) and (2).

$$\eta = \frac{3}{\phi_s} \left(\frac{1}{\tanh \phi_s} - \frac{1}{\phi_s} \right) \quad (1)$$

$$\phi_s = R \sqrt{\frac{K_1}{D_e}} \quad (2)$$

where K_1 is the first-order kinetic constant (s^{-1}), R is the sphere radius (cm), and D_e is the effective diffusion coefficient ($cm^2 s^{-1}$). Based on equations (1) and (2), a higher D_e and shorter R can achieve a better η value. The effective diffusion coefficient (D_e), based on Fick's law, is mainly related to geometrical pore properties including void fraction (θ) and tortuosity factor (τ) [68, 69]. Furthermore, the hollow structure can provide a driving force due to concentration differences at internal and external surfaces, improving the permeation rate of reactants into solid catalysts [55–61]. Therefore, the desired architectural features, such as a hollow interior, mesoporous channels, free space around catalytic sites, short seepage distance, and well-shaped morphology, are essential for achieving a high effectiveness factor (η) for the catalyst.

Accordingly, solid amines with characteristic architectural features suitable for a high effectiveness factor (η) were prepared through four steps, as shown in **Scheme 1**. First, the EGDMA-cross-linked copolymers of styrene and monomers 1a–c were coated on the surface of PS nanospheres to form core-shelled PS@PS-NH₃/OR OPNs. After the PS core was etched by THF, hollow nanospheres with a thin shell, denoted as PS-NH₃/OR HOPNs, were fabricated. Mesopore-forming acid templates 1a–c attached to the shell were then eluted with aqueous NaOH solution to imprint free space around the amine site in hollow mesoporous nanobowls PS-NH₂ HMOPBs. Finally,

PS-NH₂ HMOPNs underwent swelling in DMF at different temperatures, followed by annealing in liquid N₂ and extraction with methanol to produce inter-connected channels between spaces around amines in the shell. The as-prepared #PS-NH₂ HMOPBNs possessed a well-shaped bowl-like morphology, hollow interior, mesoporous channel, free space around amines and a thin shell, which provided the characteristic architectural features to achieve the fast mass transfer of reactants in solid base catalysis.

3.1.1. Well-shaped nanobowl with thin shell and hollow interior

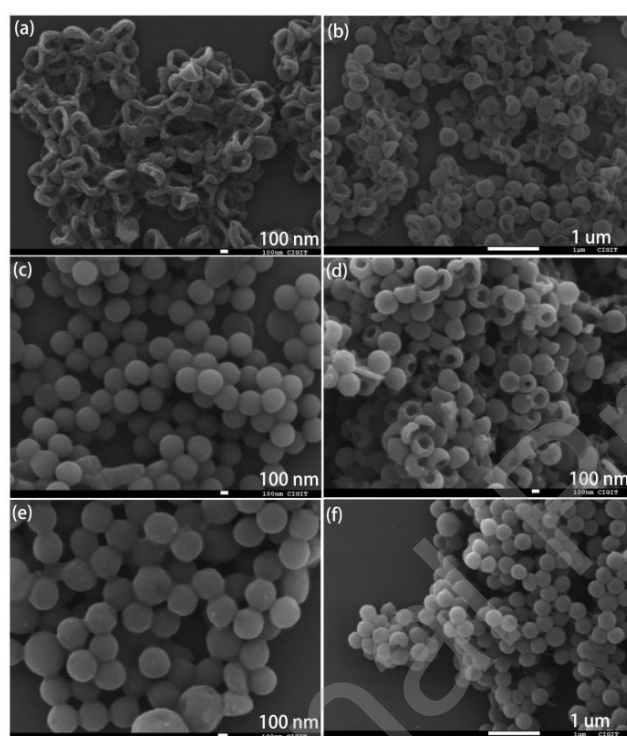


Fig.1. SEM images of PS-NH₃/OR HOPNs in DMSO/H₂O (a: 2.5:1;c: 1:1), PS-NH₂ HMOPBs in DMSO/H₂O (b: 1:2.5; d: 1:1), DVB-cross-linked PS-NH₃/OR HOPNs (e), and PS-NH₂ HMOPBs (f).

The effect of the mixed solvent volume ratio and different cross-linkers on the shell thickness and morphology of solid amines was investigated in detail. The SEM images and particle size distributions of core-shelled PS@PS-NH₃/OR OPNs are shown in **Fig. S2**. When the DMSO/H₂O volume ratio was 2.5:1.0, the obtained core-shelled PS@PS-NH₃/OR OPNs had a very thin outer shell, only about several nanometers in thickness (**Fig. S2d**). With decreasing DMSO/H₂O volume ratio from 2.5:1 to 1:1 and 1:2.5, the outer shell thickness increased to 30 nm (**Fig.**

S2e) and 29 nm (**Fig. S2f**), respectively. This indicated that the emulsion model with more monomers around the PS core was favored at a lower volume ratio of DMSO to H₂O, with the thicker outer shell coated on the PS core surface [59]. However, fewer monomers of **1a** were loaded on the PS surface, as determined by elemental analysis of nitrogen and sulfur contents, owing to the poorer dispersion of monomer **1a** in the DMSO/H₂O (1:2.5, v/v) mixed solvent. The mixed DMSO/H₂O solvent at 1:1 (v/v) was the best solvent for the formation of a thicker polymeric shell with a higher content of **1a** on the PS core. After the PS cores were removed by THF, the obtained thin shell of the hollow PS-NH₃/OR HOPNs could not provide sufficient support to balance the combined actions of centrifugal force (FC) and osmotic pressure (OP) toward the interior. Therefore, the original spherical morphology (**Fig. S2a**) was deformed into a bowl-like morphology with no void owing to the overlap of two semi-shells (**Fig. 1a**). Owing to the higher shell thicknesses of 30 and 29 nm, hollow PS-NH₃/OR HOPNs retained the original spherical morphology (**Figs. 1c** and **S3**). After imprinted molecule **1a'** in the shell was etched by aqueous NaOH solution, the released free spaces weakened the support force of the shell. Therefore, spherical PS-NH₃/OR HOPNs were observed to deform into well-shaped bowl-like PS-NH₂ HMOPBs (**Figs. 1b** and **d**). To strengthen the support force of the shell, divinylbenzene (DVB) was used instead of EGDMA as a cross-linker to enhance the shell rigidity. As expected, before and after the removal of **1a'**, the same well-shaped spherical morphology remained (**Figs. 1e** and **1f**). Furthermore, hollow interiors were clearly observed in both bowl-like PS-NH₂ HMOPBs and DVB-cross-linked nanospheres (**Fig. 2**). Therefore, the as-fabricated solid base with architectural features, including a thin shell, hollow interior, and well-shaped morphology, provided a short transmission distance (30 nm) for reactants, concentration difference-driven force, and textural uniformity to achieve a high effectiveness factor (η).

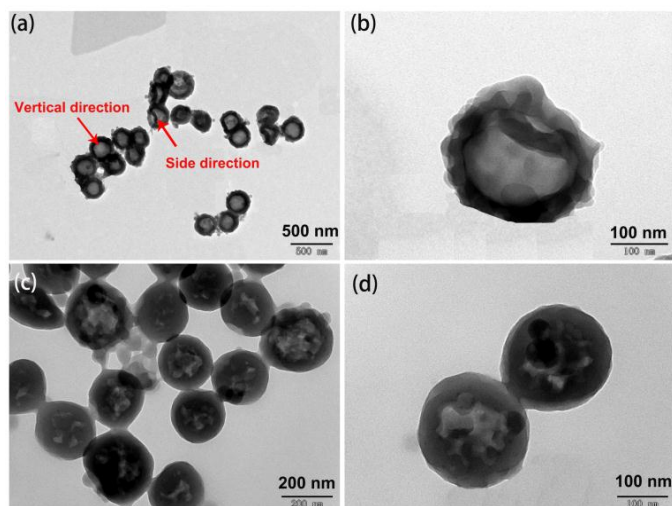


Fig.2. TEM images of (a, b) EGDMA-cross-linked PS-NH₂ HMOPBs, and (c, d) DVB-cross-linked nanospheres.

3.1.2. Free space around amine site.

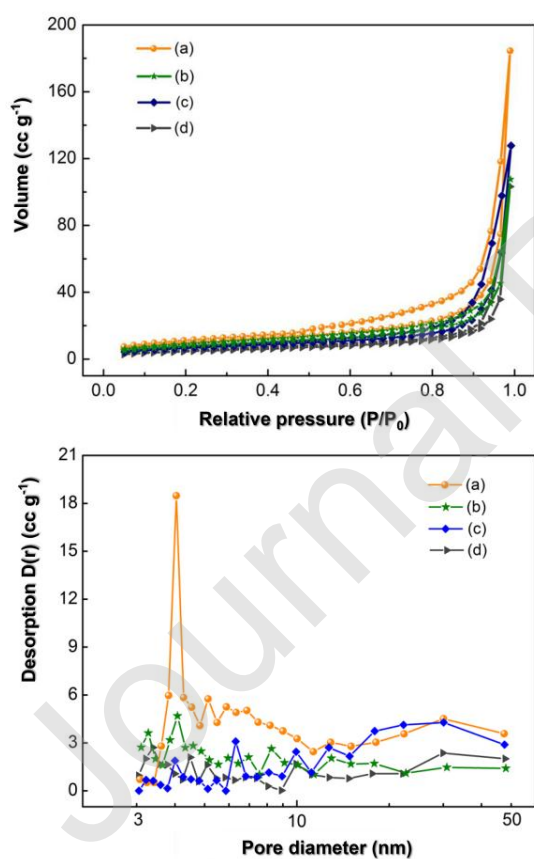


Fig.3. N₂ adsorption-desorption isotherms (upper) and pore diameter distributions (bottom) of (a) PS-NH₂ HMOPBs, (b) PS@PS-NH₃/OR OPNs, (c) PS-NH₃/OR HOPNs, and (d) DVB-cross-linked PS-NH₂ HMOPBs.

Generally, catalytic sites embedded in the solid support framework result in the poor accessibility of reactants

to the catalytic site surface. Imprinting free space around the catalytic site could effectively improve the catalytic activity in acid catalysis [63]. Herein, bulky organic acids 1a–c were used as templates to imprint free spaces around amine sites. As shown in **Fig. 3** and **Table S1**, core-shelled PS@PS-NH₃/OR OPNs in the absence of mesopore (**Fig. 3b**) were found to possess a very low surface area (9.7 m² g⁻¹) and low pore volume (0.10 cm³ g⁻¹). After removing PS, the surface area and pore volume increased to 26.9 m² g⁻¹ and 0.15 cm³ g⁻¹, respectively, owing to the formation of a hollow interior and slight increase in mesopores with pore sizes in the range of 15–50 nm (**Fig. 3c**). Interestingly, when imprinted molecules 1a', attached to the framework *via* acid–base reaction, were etched by aqueous NaOH solution, new emerging mesopores with pore sizes in the range of 3.5–10 nm, centered at 4.0 nm were obtained with the release 1a' (**Fig. 3a**). Meanwhile, the specific surface area and pore volume of PS-NH₂ HMOPBs increased to 41.3 m² g⁻¹ and 0.21 cm³ g⁻¹, respectively. When replacing cross-linker EGDMA with DVB, the as-prepared PS-NH₂ HMOPBs showed a similar trend in pore size distributions (**Fig. S7**). Unfortunately, owing to the skeleton rigidity of DVB, the DVB-cross-linked PS-NH₂ HMOPBs displayed a lower surface area (21.9 m² g⁻¹) and pore volume (0.09 cm³ g⁻¹) compared with EGDMA-cross-linked PS-NH₂ HMOPBs. These results indicated that the etching of acid 1a' could imprint free spaces around amine sites.

To enhance the imprinted free spaces around amine sites, acids 1b' and 1c' with three-dimensional structures, instead of two-dimensional acid 1a', were used as bulky templates to imprint larger free spaces. Unfortunately, owing to the difficulty in eluting bulky 1b' and 1c' from the shells completely, the as-fabricated spherical PS-NH₂ HMOPBs (**Fig. S5**) failed to achieve the desired surface areas (24.2 m² g⁻¹ and 18.8 m² g⁻¹, respectively), pore volume (0.17 cm³ g⁻¹ and 0.10 cm³ g⁻¹, respectively), and imprinted free space around the amines (**Fig. S8**). In particular, after the salts of etched molecules 1a'-c' in NaOH solution were acidified and purified by column chromatography, organic acids 1a'-c' could be reused to prepare amine salts 1a-c.

3.1.3. Mesoporous channels

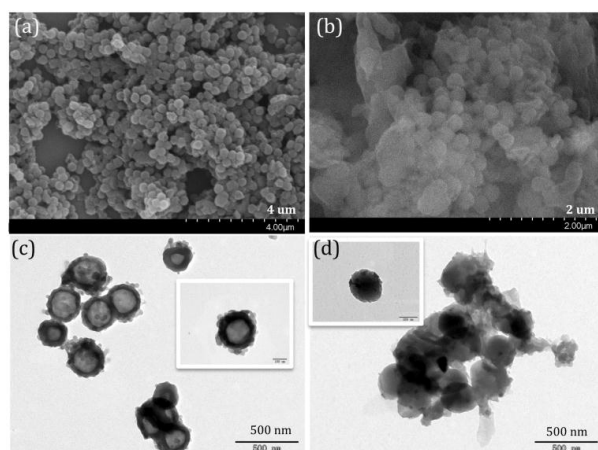


Fig.4. SEM and TEM images of #PS-NH₂ HMOPBs prepared at DMF swelling temperatures of (a, c) 80 °C, and (b, d) 115 °C.

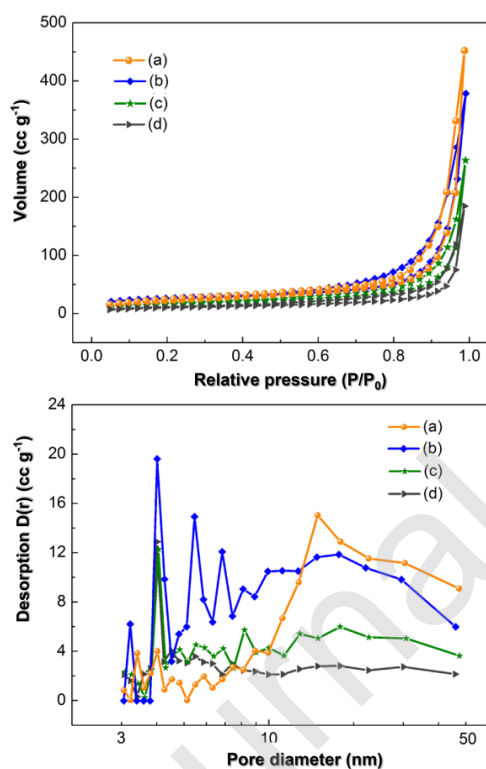


Fig.5. N₂ adsorption-desorption isotherms (upper) and pore diameter distributions (bottom) of (d) PS-NH₂ HMOPBs and #PS-NH₂ HMOPBs at different swollen temperatures of (a) 145 °C, (b) 115 °C, and (c) 80 °C.

We attempted to construct mesoporous channels in the shells of PS-NH₂ HMOPBs to connect free spaces around bases using a Co(OAc)₂-templated method [50, 63]. Unfortunately, no improvement in surface area (22.2 m² g⁻¹) and pore volume (0.14 cm³ g⁻¹) was observed. Based on the known swelling behavior of polystyrene in DMF

at high temperature, and the formation of a mesoporous network after removal of crystalline DMF by MeOH at cryogenic temperatures [64], hollow mesoporous #PS-NH₂ HMOPBs with a well-shaped hollow morphology were fabricated, and the specific surface areas and pore volumes were improved. From the SEM (**Fig. 4a**) and TEM (**Fig. 4c**) images, #PS-NH₂ HMOPBs(80), prepared using a DMF swelling temperature of 80 °C, possessed the original hollow interior and well-shaped bowl-like morphology. The specific surface area and pore volume increased from 41.3 m² g⁻¹ and 0.21 cm³ g⁻¹ to 56.5 m² g⁻¹ and 0.41 cm³ g⁻¹, respectively. In particular, the desorption D(r) of mesopores in the range of 5–50 nm was significantly enhanced (**Fig.5c**), indicating that the mesoporous channels had newly emerged in the shell. At a DMF swelling temperature of 115 °C, some #PS-NH₂ HMOPBs(115) were observed to collapse and lose the original well-shaped morphology and hollow interior (**Figs. 4b and 4d**). However, the specific surface area and pore volume increased to 66.3 m² g⁻¹ and 0.45 cm³ g⁻¹, and mesopores in the range of 3–50 nm were also significantly increased (**Fig. 5b**). Upon further increasing the DMF swelling temperature to 145 °C, the obtained #PS-NH₂ HMOPBs(145) exhibited the highest specific surface area (84.1 m² g⁻¹) and pore volume (0.51 cm³ g⁻¹). Frustratingly, all nanoparticles of #PS-NH₂ HMOPBs(115) collapsed and lost their well-shaped morphology and hollow structure (**Fig. S6**). Furthermore, mesopores with pore diameters of 3–10 nm were significantly reduced, while mesopores with pore diameters of 10–50 nm further increased (**Fig.5a**), indicating that the mesoporous structure was destroyed owing to excessive spinodal decomposition of the polymeric shell [64]. Based on these results, N₂ annealing was considered as a method to effectively improve the specific surface area and pore volume, and produce mesoporous channels to connect the free spaces around amine sites. Considering these integrated factors, such as morphology and porosity, the optimal DMF swelling temperature for PS-NH₂ HMOPBs was concluded to be 80 °C, at which the mesoporous channels (5–50 nm) in the shell of #PS-NH₂ HMOPBs(80) were constructed and could connect free spaces around base sites.

3.2. Architectural features of various solid amines



Fig.6. Architectural features of various catalysts: (a) PS-NH₂ OPNs, (b) PS-NH₂ HOPNs, (c) PS-NH₂ HMOPBs, (d) #PS-NH₂ HMOPBs(80), (e) #PS-NH₂ HMOPBs(115), and (f) #PS-NH₂ HMOPBs(145).

To clarify the vital functions of architectural features, such as the hollow interior, free spaces around base sites, and inter-connected mesoporous channels, in catalysis, solid amines, solid PS-NH₂ OPNs and hollow PS-NH₂ HOPNs, were prepared as contrast catalysts according to the procedures shown in **Scheme S1**. The main differences among these catalysts were the architectural features, including morphology and porosity (**Fig. 6**). PS-NH₂ OPNs with a mean particle size of 79 nm were solid, while PS-NH₂ HOPNs with a mean particle size of 314 nm were hollow. Both solid amines had low specific areas and pore volumes. By imprinting free spaces around the amine sites in the shell of hollow PS-NH₂ HOPNs, more amine sites in PS-NH₂ HMOPBs were exposed to reactants due to imprinted free spaces around base sites centered at 4.0 nm. Interestingly, after PS-NH₂ HMOPBs were swollen in DMF, annealed in liquid N₂, and extracted by methanol to remove frozen DMF, more mesopores were constructed in #PS-NH₂ HMOPBs at DMF swelling temperatures of 80, 115, and 145 °C. The porosity in the shell of #PS-NH₂ HMOPBs(80), obtained at 80 °C, comprised the original free spaces around amine sites, centered at 4.0 nm, and newly emerged mesoporous channels (5–50 nm). Upon increasing the DMF swelling temperature to 115 °C, all mesopores (3–50 nm) in #PS-NH₂ HMOPBs(115) were significantly increased. At DMF swelling temperature of 145 °C, mesopores (3–10 nm) were significantly reduced, while mesopores (10–50 nm) were further increased (**Fig.**

5). Furthermore, the specific surface areas and pore volumes of #PS-NH₂ HMOPBs increased with increasing DMF swelling temperature. Notably, the well-shaped nanobowls gradually collapsed into floccus solids at DMF swelling temperatures above 115 °C, with free spaces around the amine sites disappearing due to excessive spinodal decomposition of the shell.

3.3. Amine loading capacity

FT-IR spectra were recorded to confirm the immobilization of benzylamine in the framework of various solid amines (**Fig. S9**). The adsorption peaks at 3483 and 3437 cm⁻¹ corresponded to symmetric and asymmetric N-H stretching vibrations in NH₂ groups. The band at 1739 cm⁻¹ was assigned to the stretching vibration of C=O in EGDMA, with the band at 1630 cm⁻¹ attributed to the flexural vibration of N-H bonds in NH₂ groups. These results indicated that benzylamine moieties had been successfully loaded onto the solid amine frameworks. According to the nitrogen contents obtained by elemental analysis, the amine loading capacities in PS-NH₂ OPNs, PS-NH₂ HOPNs, and PS-NH₂ HMOPBs were calculated to be 0.70, 0.60, and 0.82 mmol g⁻¹, respectively.

3.4. Catalytic activity in Knoevenagel condensation

Based on the inherent functions of amines, the as-fabricated well-shaped solid amines with hollow interiors, mesoporous channels and thin shells have extensive potential applications, including in base catalysis, metal coordination chemistry, and carbon capture in environmental science. Therefore, the Knoevenagel condensation of benzaldehyde with malononitrile was selected as a model reaction to investigate the improved activity of solid amines in heterogeneous base catalysis.

3.4.1. Optimization of reaction parameters

Table 1

Knoevenagel condensation of benzaldehyde with malononitrile catalysed by PS-NH₂ HMOPBs under different

conditions.^a

Entry	Cat. (g/mol%)	Solvent	Temp. (°C)	Yield (%) ^b
1	61/5.0	Toluene	15	89
2	61/5.0	Toluene	25	92
3	61/5.0	Toluene	40	92
4	61/5.0	Toluene	60	93
5	61/5.0	Acetonitrile	25	89
6	61/5.0	CH ₂ Cl ₂	25	80
7	61/5.0	Ethanol	25	98
8	61/5.0	THF	25	91
9	37/3.0	Ethanol	25	93
10	12/1.0	Ethanol	25	86

^a Reaction conditions: benzaldehyde (106.0 mg, 1.0 mmol), malononitrile (79.0 mg, 1.2 mmol), 2 mL of solvent, 3 h.

^b Isolated yield.

Using PS-NH₂ HMOPBs as the base catalyst, the effects of different parameters, such as temperature, solvent, and amount of solid base, on the Knoevenagel condensation of benzaldehyde with malononitrile were investigated, with the results shown in **Table 1**. At 25, 40, and 60 °C, similar yields were obtained. Therefore, with regard to energy consumption, 25 °C was selected as the optimum reaction temperature. PS-NH₂ HMOPBs afforded the highest product yield (98%) in ethanol, indicating that polar protic solvents were favorable for the Knoevenagel condensation. When the amount of solid amine used was decreased from 5 mol% to 3 and 1 mol%, the yield decreased from 98% to 93 and 86%, respectively. According to these results, 5 mol% of PS-NH₂ HMOPBs in ethanol at 25 °C were considered the optimum reaction conditions for subsequent reactions.

3.4.2. Effects of porosity and morphology.

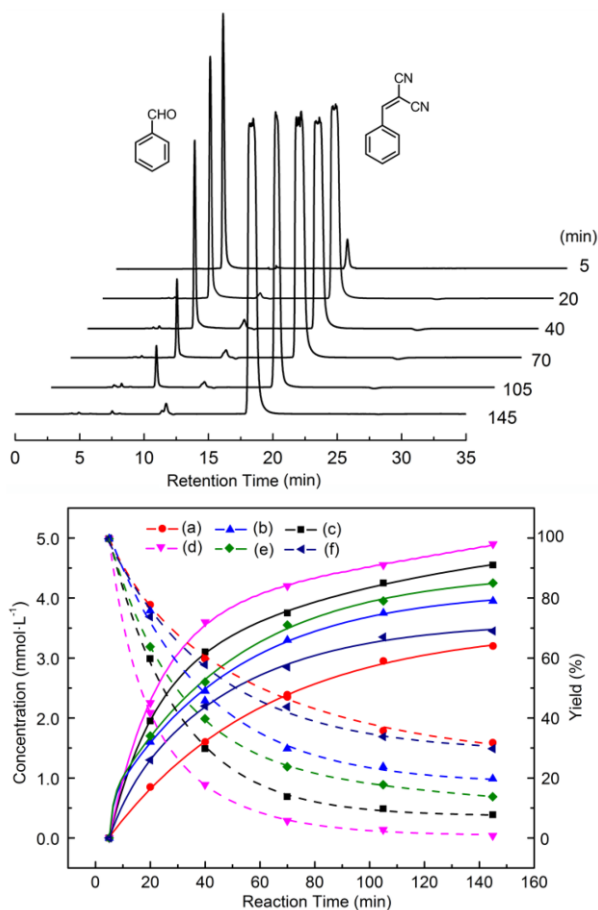


Fig.7. HPLC monitoring of Knoevenagel condensation promoted by #PS-NH₂ HMOPBs (80) (top), and concentrations and yields of product versus reaction times (bottom) catalyzed by various solid amines: (a) PS-NH₂ OPNs, (b) PS-NH₂ HOPNs, (c) PS-NH₂ HMOPBs, (d) #PS-NH₂ HMOPNs(80), (e) #PS-NH₂ HMOPBs (115), and (f) #PS-NH₂ HMOPNs (145).

Under the optimized conditions, the Knoevenagel condensation of benzaldehyde with malononitrile was used as a model reaction to investigate the morphology- and mesopore-dependent catalytic activities of solid amines. The Knoevenagel condensation reactions, promoted by various solid amines, were monitored throughout by HPLC (**Fig. S10–S14**). The benzaldehyde concentrations and product yields were plotted versus reaction times, as shown at the bottom of **Fig. 7**. According to the benzaldehyde concentration as a function of reaction time, the relationship between concentration (mmol L⁻¹) and reaction time (min) could be expressed as follows:

PS-NH₂ OPNs (a):

$$c_a = 14/t + 2.2 \quad (R^2=0.998)$$

PS-NH₂ HOPNs (b):

$$c_b = 19/t + 1.2 \quad (R^2=0.992)$$

PS-NH₂ HMOPBs (c):

$$c_c = 23/t + 0.40 \quad (R^2=0.999)$$

#PS-NH₂ HMOPBs(80) (d):

$$c_d = 25/t + 0.60 \quad (R^2=0.996)$$

#PS-NH₂ HMOPBs(115) (e):

$$c_e = 21/t + 0.80 \quad (R^2=0.990)$$

#PS-NH₂ HMOPNs(145) (f):

$$c_f = 15/t + 2.0 \quad (R^2=0.999)$$

The derivative of concentration versus time was considered to be the reaction rate of benzaldehyde at a certain time. The initial reaction rate of benzaldehyde at 20 min was selected as a parameter for evaluating the catalytic activity of solid amine. Therefore, $d[c_a]/dt = 14/t^2$, $d[c_b]/dt = 19/t^2$, $d[c_c]/dt = 23/t^2$, $d[c_d]/dt = 25/t^2$, $d[c_e]/dt = 21/t^2$, and $d[c_f]/dt = 15/t^2$. At 20 min, the initial reaction rates of the various solid bases were calculated to be 35.0, 47.5, 57.5, 62.5, 52.5, and 37.5 mmol L⁻¹ min⁻¹, respectively. The reaction rates were shown to be directly related to the architectural features of solid amines. Solid PS-NH₂ OPNs displayed the lowest catalytic activity owing to the low specific surface area (17.1 m² g⁻¹) and pore volume (0.15 cm³ g⁻¹) (**Fig. 7a**). After the PS-templated hollow interior was fabricated, the hollow interior in PS-NH₂ HOPNs produced a driving force owing to the internal–external concentration difference, with the initial reaction rate increasing from 35.0 to 47.5 mmol L⁻¹ min⁻¹ (**Fig. 7b**). As expected, upon imprinting the free spaces around –NH₂ sites, the initial reaction rate of PS-NH₂ HMOPNs increased to 57.5 mmol L⁻¹ min⁻¹ (**Fig. 7c**), which was attributed to the easy accessibility of reactants to exposed –NH₂ sites.

The interconnected mesoporous channels in the shell, constructed by solvent annealing of the DMF-swollen solid base, improved the accessibility of reactants to the $-\text{NH}_2$ sites. The as-obtained #PS- NH_2 HMOPNs(80) with an increased specific surface area ($56.5 \text{ m}^2 \text{ g}^{-1}$) and pore volume ($0.41 \text{ cm}^3 \text{ g}^{-1}$) showed the highest initial reaction rate ($62.5 \text{ mmol L}^{-1} \text{ min}^{-1}$) (**Fig. 7d**). When the DMF-swollen temperature was increased to 115 and 145 °C, the specific surface areas and pore volumes of #PS- NH_2 HMOPNs(115) and #PS- NH_2 HMOPNs(145) further increased to $66.3 \text{ m}^2 \text{ g}^{-1}$ and $0.45 \text{ cm}^3 \text{ g}^{-1}$, and $84.1 \text{ m}^2 \text{ g}^{-1}$ and $0.51 \text{ cm}^3 \text{ g}^{-1}$, respectively. Unfortunately, both solid amines showed inferior catalytic activities. The initial reaction rate of #PS- NH_2 HMOPNs(115) decreased to $52.5 \text{ mmol L}^{-1} \text{ min}^{-1}$ (**Fig. 7e**), resulting from damage to the free spaces around $-\text{NH}_2$ sites (**Fig. 5b**) and the hollow interior (**Fig. 4d**). At the DMF-swollen temperature of 145 °C, the initial reaction rate of as-prepared #PS- NH_2 HMOPNs(145) sharply decreased to $37.5 \text{ mmol L}^{-1} \text{ min}^{-1}$ (**Fig. 7f**). From the FT-IR spectrum of #PS- NH_2 HMOPNs(145) (**Fig. S9c**), the newly emerged N-H bending vibration at 1670 cm^{-1} indicated that some $-\text{NH}_2$ groups reacted with the carboxylic ester in EGDMA to form the corresponding amides. Meanwhile, a strong decrease in mesopores below 10 nm and complete collapse of the well-shaped nanobowls into floccus solids were observed using the pore size distribution (**Fig. 5a**) and SEM and TEM images (**Fig. S6**). These three factors unfavorable to the mass transfer of reactants and reactivity of $-\text{NH}_2$ sites resulted in a sharp decrease in the catalytic activity of #PS- NH_2 HMOPNs(145).

3.4.3. Scope of Knoevenagel condensations

Table 2 Knoevenagel condensation reactions of aromatic aldehydes and malononitrile catalyzed by #PS- NH_2 HMOPBs(80) and PS- NH_2 HMOPBs.^a

Entry	Cat.	R	Time (h)	Conv. (%) ^b	Yield (%) ^c
1	A ^d	2-NO ₂	3	>99	82

	B ^e		2	>99	85
	B ^f		2	>99	96
2	A ^d	3-NO ₂	3	>99	82
	B ^e		2	>99	86
3	A ^d	4-NO ₂	3	>99	96
	B ^e		2	>99	96
4	A ^d	2-OCH ₃	3	96	92
	B ^e		2	98	93
5	A ^d	3-OCH ₃	3	98	94
	B ^e		2	99	95
6	A ^d	2-CH ₃	3	99	95
	B ^e		2	>99	96
7	A ^d	3-CH ₃	3	>99	97
	B ^e		2	>99	98
8	A ^d	4-CH ₃	3	>99	94
	B ^e		2	>99	96
9	A ^d	2-Cl	3	>99	81
	B ^e		2	>99	84
	B ^f		2	>99	95
10	A ^d	3-Cl	3	>99	80
	B ^e		2	>99	85
11	A ^d	4-Cl	3	>99	79

	B ^e		2	>99	85
12	A ^d	H	3	>99	98
	B ^e		2	>99	98

^a Reaction conditions: benzaldehyde (106.0 mg, 1.0 mmol), malononitrile (79.0 mg, 1.2 mmol), Cat. (61.0 mg, 5 mol%), 2 mL of ethanol, 25 °C.

^b Determined by HPLC.

^c Isolated yield.

^d A: PS-NH₂ HMOPBs.

^e B: #PS-NH₂ HMOPNs(80).

^f Toluene as solvent.

Encouraged by the excellent catalytic activities of #PS-NH₂ HMOPNs(80) at 25 °C, the scope of Knoevenagel condensation was broadened to various aromatic aldehydes. The catalytic results are summarized in **Table 2**. Except for *p*-NO₂-C₆H₄CHO, the aromatic aldehydes bearing electron-withdrawing groups, such as nitro (-NO₂) and chloro (-Cl) groups attached to the *o*-, *m*- and *p*-positions of phenyl were less reactive in ethanol, producing the corresponding products in only 76%–86% yields, despite high conversions of the aromatic aldehydes (>99%). These results were inconsistent with previously reported results [70–72,20,21,23,26]. When the temperature was increased to 60 °C, the yields were not significantly improved. Fortunately, high yields of above 95% were achieved in toluene (**Table 2**, entries 1 and 9). Aromatic aldehydes bearing electron-withdrawing groups were speculated to react with ethanol to form corresponding hemiacetals, which resulted in the decreased yields. For aromatic aldehydes containing electron-donating groups, such as *o*-, *m*-, or *p*-OCH₃ and -CH₃, high yields (92-98%) were obtained at room temperature. Knoevenagel condensations at room temperature that afforded high yields in short reaction times using a low catalyst loading (5 mol%) were attributed to the comprehensive effect of thin shells, free space around

the amine sites and mesoporous channels of hollow #PS-NH₂ HMOPNs(80) and PS-NH₂ HMOPNs.

3.4. Catalyst reusability and restoration

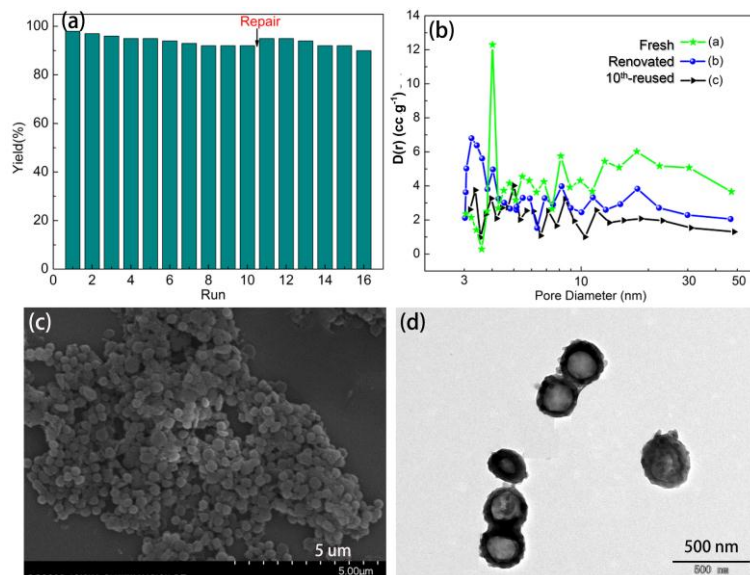


Fig.8. Reusability (a) of #PS-NH₂ HMOPBs (80), pore diameter distribution (b) of fresh, 10th-reused, and restored #PS-NH₂ HMOPBs(80), SEM (c) and TEM (d) images of 10th-reused #PS-NH₂ HMOPBs(80).

The reusability of #PS-NH₂ HMOPBs(80) and PS-NH₂ HMOPBs in the Knoevenagel condensation of benzaldehyde and malononitrile was investigated under the optimized conditions. When the Knoevenagel condensation was determined to be complete by TLC monitoring, the catalyst was separated by centrifugation, washed several times with ethanol, and reused directly in the next catalytic cycle. The yields are shown in **Fig. 8a** and **Table S3**. As shown in **Fig. 8a**, #PS-NH₂ HMOPBs(80) showed higher yields than PS-NH₂ HMOPBs until the tenth run. However, a small decrease was observed in the yield from the first run (98% and 98%) to the tenth run (92% and 89%), for #PS-NH₂ HMOPBs(80) and PS-NH₂ HMOPBs, respectively. Using #PS-NH₂ HMOPBs(80) as an example, N₂ adsorption–desorption isotherm, SEM, and TEM were used as tools to explain the decreased yield. The SEM and TEM images showed that #PS-NH₂ HMOPNs(80) reused ten times maintained the original bowl-like morphology (**Fig. 8c**) and hollow interior (**Fig. 8d**). The N₂ adsorption–desorption isotherm of #PS-NH₂ HMOPNs(80) reused ten times showed that the D(r) values of the mesopores (3–50 nm) were significantly decreased

(**Fig. 8b**), and that the specific surface area and pore volume decreased to $25.6 \text{ m}^2 \cdot \text{g}^{-1}$ and $0.08 \text{ cm}^3 \cdot \text{g}^{-1}$, respectively. Therefore, the decreased yields were speculated to be attributed to blockage of the mesopores, resulting in the poorer mass transfer of reactants. The removal of plugging material was an effective and convenient strategy for restoring the catalytic activity of #PS-NH₂ HMOPNs(80). The catalyst (100 mg) reused for the tenth time was allowed to stir in HCl-containing (1.0 mol L^{-1}) aqueous ethanol solution (1/1, v/v) at room temperature for 12 h and separated by centrifugation. HPLC spectra indicated that the yellow centrifugate contained a large number of ylidenemalononitriles, confirming that the bulky product clogged mesopores in the shell. After isolated #PS-NH₂ HMOPNs(80) was neutralized by NaOH-containing aqueous ethanol solution at room temperature for 12 h, the specific surface area and pore volume of #PS-NH₂ HMOPNs(80) were refreshed to $41.8 \text{ m}^2 \cdot \text{g}^{-1}$ and $0.25 \text{ cm}^3 \cdot \text{g}^{-1}$, and the mesopores (3–50 nm) were reconstructed (**Fig. 8b**). As expected, the catalytic activity of solid amines was restored to achieve a high yield (96%) similar to a fresh solid amine catalyst. In the subsequent six runs, high yields above 90% were obtained (**Fig. 8a**).

4. Conclusions

In heterogeneous catalysis, chemical catalytic reactions are conducted at the surface of catalytically active sites. Pore-, size-, and morphology-dependent factors, such as mesopores, hollow interior, and transmission thickness, are keys to the accessibility of reactants to catalytic sites. Herein, the other contributors to mass transfer, namely, free spaces around base sites and interconnected mesoporous channels, were designed and applied to Knoevenagel condensation. Through etching the PS core in the interior and the attached organic acid in the shell to release their occupied spaces, and construction of mesoporous channels via swelling in DMF, annealing in liquid N₂, and frozen DMF removal, nanobowls with desired architectural features, such as hollow interior, free spaces around amine sites, and interconnected mesoporous channels, were fabricated to effectively improve the accessibility of reactants

to the surface of base sites. The as-fabricated amine-functionalized hollow nanobowl-like solid base promoted Knoevenagel condensations of various aromatic aldehydes with malononitrile at room temperature in high yields. Furthermore, the solid base possessed good reusability, and was restored using aqueous HCl solution to achieve the original high catalytic activity. Therefore, the construction of free spaces around the base site and interconnected mesoporous channels between them, is an effective and facile method for fabricating permeable skeleton structures in polymeric amine base catalysts to achieve fast mass transfer in the catalytic process. The nanobowl-like hollow solid amine base with imprinted free spaces around catalytic sites and interconnected mesopores is believed to have high potential in heterogeneous base catalysis. The new concept of the construction of free space around the catalytic site and mesoporous channel to access catalytic sites is of interest in environmental sciences, such as coordination chemistry and carbon capture. To further improve this strategy, possible future directions include: (i) Accurate control of the volume of free room around amine sites; (ii) the preparation of more rigid and stable polymeric skeletons suitable for pore maintenance; and (iii) investigations into the applicable scope for other organic base.

CRedit author statement

Li Zhang: Data curation, Visualization, Investigation. **Jianing Zhang:** Formal analysis, Software. **Shuai Wei:** Validation, Resources. **Shan Li:** Resources. **Xuebing Ma:** Conceptualization, Methodology, Writing-Reviewing and Editing, Project administration, Funding acquisition.

Declaration of interests

No.

Acknowledgements

This work was supported by National Natural Science Foundation of China [51973177], and Basic Science and Advanced Technology Research Project of Chongqing Science&Technology commission, P. R. China (cstc 2017jcyjBX0027). We thank Simon Partridge, PhD, from Liwen Bianji, Edanz Editing China

(www.liwenbianji.cn/ac), for editing the English text of a draft of this manuscript.

Supplementary data

Characterizations of solid bases such as FT-IR, SEM, TEM and N₂ adsorption–desorption isotherms, data of products such as ¹H NMR and synthetic procedures of monomers and contrast solid bases can be found, in the online version, at.....

References

- [1] H. Hattori, *Appl. Catal. A, Gen.* 504 (2015) 103–109.
- [2] S. Ramesh, F. Devred, D. P. Debecker, *Appl. Catal. A, Gen.* 581 (2019) 31–36.
- [3] S. S. Peng, J. K. Wu, A. Z. Peng, Y. X. Li, C. Gu, M. B. Yue, X. Q. Liu, L. B. Sun, *Appl. Catal. A, Gen.* 584 (2019) 117153.
- [4] X. Jin, J. Shen, W. J. Yan, M. Zhao, P. S. Thapa, B. Subramaniam, R. V. Chaudhari, *ACS Catal.* 5 (2015) 6545–6558.
- [5] L. Zhu, X. Q. Liu, H. L. Jiang, L. B. Sun, *Chem. Rev.* 117 (2017) 8129–8176.
- [6] Wenlei Xie Fei Wan, *Energ. Convers. Manage.* 198(2019)111922.
- [7] W. L. Xie, F. Wan, *Fuel* 220 (2018) 248–256.
- [8] Y. X. Han, H. Y. Wang, *Renew. Energ.* 125 (2018) 675–681).
- [9] A. Marwaha, A. Dhir, S. K. Mahla, S. K. Mohapatra, *Catal. Rev.* 60 (2018) 594–628.
- [10] M. Pelckmans, T. Renders, S. Van de Vyver, B. F. Sels, *Green Chem.* 19 (2017) 5303–5331.
- [11] T. Kano, K. Maruoka, *Chem. Sci.* 4 (2013) 907–915.
- [12] P. Melchiorre, *Angew. Chem., Int. Ed.* 51 (2012) 9748–9770.
- [13] P. Bhattacharya, D. E. Prokopchuk, M. T. Mock, *Coordin. Chem. Rev.* 334 (2017) 67–83.

- [14] L. Fabbrizzi, A. Poggi, *Chem. Soc. Rev.* 42 (2013) 1681–1699.
- [15] W. Z. Wang, Y. C. Xu, L. Wang, L. L. Li, L. Xia, X. G. Jia, G. H. Lee, S. M. Peng, *J. Mol. Struct.* 1193 (2019) 280–285.
- [16] X. J. Chen, G. Huang, C. J. An, Y. Yao, S. Zhao, *Chem. Eng. J.* 335 (2018) 921–935.
- [17] X. Yang, R. J. Rees and W. Conway, G. Puxty, Q. Yang, D. A. Winkler, *Chem. Rev.* 117 (2017) 9524–9593.
- [18] H. M. Stowe, G. S. Hwang, *Ind. Eng. Chem. Res.* 56 (2017) 6887–6899.
- [19] L. Zhu, X. Q. Liu, H. L. Jiang, L. B. Sun, *Chem. Rev.* 117 (2017) 8129–8176.
- [20] B. Sakthivel, A. Dhakshinamoorthy, *J. Colloid Interf. Sci.* 485 (2017) 75–80.
- [21] B. Xue, J. G. Zhu, N. Liu, Y. X. Li, *Catal. Commun.* 64 (2015) 105–109.
- [22] J. Xu, K. Shen, B. Xue, Y. X. Li, *J. Mol. Catal. A: Chemical* 372 (2013) 105–113.
- [23] H. H. Jia, Y. Zhao, P. P. Niu, N. Y. Lu, B. B. Fan, R. F. Li, *Mol. Catal.* 449 (2018) 31–37.
- [24] G. B. Varadwaj, S. Rana, K. M. Parida, *Dalton Trans.* 42 (2013) 5122–5129.
- [25] J. Shabir, C. Garkoti, Surabhi, D. Sah, S. Mozumdar, *Catal. Lett.* 148 (2018) 194–204.
- [26] Y. B. Sun, C. Y. Cao, P. P. Huang, S. L. Yang, W. G. Song, *RSC Adv.* 5 (2015) 86082–86087.
- [27] F. Xue, H. He, H. X. Zhu, H. H. Huang, Q. Wu, S. F. Wang, *Langmuir* 35 (2019) 12636–12646.
- [28] M. J. Lashaki, S. Khiavi, A. Sayari, *Chem. Soc. Rev.* 48 (2019) 3320–3405.
- [29] A. J. Emerson, A. Chahine, S. R. Batten, D. R. Turner, *Coord. Chem. Rev.* 365 (2018) 1–22.
- [30] S. Gadipelli, Y. Lu, N. T. Skipper, T. Yildirim, Z. X. Guo, *J. Mater. Chem. A* 5 (2017) 17833–17840.
- [31] S. Matera, W. F. Schneider, A. Heyden, A. Savara, *ACS Catal.* 9 (2019) 6624–6647.
- [32] L. Pirro, P. S. F. Mendes, S. Paret, B. D. Vandegehuchte, G. B. Marin, J. M. Thybaut, *Catal. Sci. Technol.* 9 (2019) 3109–3125.
- [33] M. Jorgensen, H. Gronbeck, *ACS Catal.* 7 (2017) 5054–5061.

- [34] K. Ge, Q. C. Yu, S. H. Chen, X. Y. Shi, J. Q. Wang, *Chem. Eng. J.* 364 (2019) 328–339.
- [35] J. Jiao, J. Cao, Y. Xia, L. Z. Zhao, *Chem. Eng. J.* 306 (2016) 9–16.
- [36] M. Afkhamipour, M. Mofarahi, *RSC Adv.* 7 (2017) 17857–17872.
- [37] R. Chakravarti, M. L. Kantam, H. Iwai, S. S. Al-deyab, K. Ariga, D. H. Park, J. H. Choy, K. S. Lakhi, A. Vinu, *ChemCatChem* 6 (2014) 2872–2880.
- [38] F. X. Zhu, D. D. Yang, F. Zhang, H. X. Li, *J. Mol. Catal. A: Chemical* 363–364 (2012) 387–397.
- [39] Y. W. Xie, K. K. Sharma, A. Anan, G. Wang, A. V. Biradar, T. Asefa, *J. Catal.* 265 (2009) 131–140.
- [40] K. Tanemura, T. Suzuki, *Tetrahedron Lett.* 59 (2018) 392–396.
- [41] P. Valvekens, M. Vandichel, M. Waroquier, V. Van Speybroeck, D. De Vos, *J. Catal.* 317 (2014) 1–10.
- [42] Y. W. Ren, J. X. Lu, O. Jiang, X. F. Cheng, J. Chen, *Chin. J. Catal.* 36 (2015) 1949–1956.
- [43] S. Z. Xing, J. Li, G. Q. Niu, Q. X. Han, J. J. Zhang, H. L. Liu, *Mol. Catal.* 458 (2018) 83–88.
- [44] A. Taher, D. J. Lee, B. K. Lee, I. M. Lee, *Synlett* 27 (2016) 1433–1437.
- [45] J. Z. Chen, R. L. Liu, H. Gao, L. M. Chen, D. Q. Ye, *J. Mater. Chem. A* 2 (2014) 7205–7213.
- [46] D. P. Yuan, N. Zhao, Y. X. Wang, K. Xuan, F. Li, Y. F. Pu, F. Wang, L. Li, F. K. Xiao, *Appl. Catal. B: Environ.* 240 (2019) 182–192.
- [47] F. J. Liu, K. Huang, A. M. Zheng, F. S. Xiao, S. Dai, *ACS Catal.* 8 (2018) 372–391.
- [48] F. J. Liu, W. P. Kong, C. Z. Qi, L. F. Zhu, F. S. Xiao, *ACS Catal.* 2 (2012) 565–572.
- [49] X. M. Zhang, L. Zhang, Q. H. Yang, *J. Mater. Chem. A* 2 (2014) 7546–7554.
- [50] G. X. Xie, S. W. Wei, L. Zhang, X. B. Ma, *Ind. Eng. Chem. Res.* 58 (2019) 2812–2823.
- [51] J. Mondal, Q. T. Trinh, A. Jana, W. K. H. Ng, P. Borah, H. Hirao, Y. L. Zhao, *ACS Appl. Mater. Interfaces* 8 (2016) 15307–15319.
- [52] V. Iablokov, Y. Z. Xiang, A. Meffre, P. F. Fazzini, B. Chaudret, N. Kruse, *ACS Catal.* 6 (2016) 2496–2500.

- [53] S. Cao, F. Tao, Y. Tang, Y. T. Li, J. G. Yu, *Chem. Soc. Rev.* 45 (2016) 4747–476.
- [54] J. H. Xu, J. Pang, D. D. Feng, X. B. Ma, *Mol. Catal.* 443 (2017) 139–147.
- [55] W. Zhu, Z. Chen, Y. Pan, R. Y. Dai, Y. Wu, Z. B. Zhuang, D. S. Wang, Q. Peng, C. Chen, Y. D. Li, *Adv. Mater.* 31 (2019) 1800426.
- [56] J. Y. Wang, J. W. Wan, D. Wang, *Acc. Chem. Res.* 52 (2019) 2169–2178.
- [57] G. X. Xie, J. N. Zhang, X. B. Ma, *ACS Catal.* 9 (2019) 9081–9086.
- [58] Z. W. Yan, G. X. Xie, J. N. Zhang, X. B. Ma, *Mol. Catal.* 464 (2019) 39–47.
- [59] Z. W. Zhao, D. D. Feng, G. X. Xie, X. B. Ma, *J. Catal.* 359 (2018) 36–45.
- [60] F. Teng, G. X. Xie, L. Zhang, X. B. Ma, *ChemCatChem* 10 (2018) 4586–4593.
- [61] G. X. Xie, J. K. Tian, S. Wei, X. Z. Liu, X. B. Ma, *Appl. Catal. A, Gen.* 565 (2018) 87–97.
- [62] M. Lehmann, M. Dechant, M. Lambov, T. Ghosh, *Acc. Chem. Res.* 52 (2019) 1653–1664.
- [63] Y. N. Bo, X. R. Wang, X. T. Deng, X. B. Ma, *Appl. Catal. A, Gen.* 590 (2020) 117360.
- [64] M. R. Krishnan, Y. C. Chien, C. F. Cheng, R. M. Ho, *Langmuir* 33 (2017) 8428–8435.
- [65] A. Sengar, J. A. M. Kuipers, R. A. V. Santen, J. T. Padding, *Phys. Rev. E* 96 (2017) 022115.
- [66] D. Cheng, S. Wang, J. A. M. Kuipers, *Chem. Eng. Sci.* 160 (2017) 80–84.
- [67] Z. P. Lu, M. M. Dias, J. C. B. Lopes, G. Carta, A. E. Rodrigues, *Ind. Eng. Chem. Res.* 32 (1993) 1839–1852.
- [68] M. Tatlier, A. Erdem-Senatalar, *Chem. Eng. J.* 102 (2004) 209–216.
- [69] F. G. HO, W. Strieder, *Chem. Eng. J.* 36 (1981) 253–258.
- [70] M. Arghan, N. Koukabi, E. Kolvari, *J. Saudi Chem. Soc.* 23 (2019) 150–161.
- [71] K. Ikeue, N. Miyoshi, T. Tanaka, M. Machida, *Catal. Lett.* 141 (2011) 877–881.
- [72] A. Pineda, A. M. Balu, J. M. Campelo, A. A. Romero, R. Luque, *Catal. Commun.* 33 (2013) 1–6.